STUDY OF STRUCTURAL, ELASTIC, ELECTRONIC, OPTICAL AND THERMAL PROPERTIES OF Ni_3Al

M. FATMI[1]*, M.A. GHEBOULI[2], B. GHEBOULI[3], T. CHIHI[4], S. BOUCETTA[4], Z.K. HEIBA[5,6]

[1] Research Unit on Emerging Materials (RUEM), University Ferhat Abbas of Setif 19000, Algeria
[2] Physics department, Universitary Center, Bordj Bou-Arreridj 34000, Algeria.
[3] Laboratory of Studies of Surfaces and Interfaces of Solids Materials, University Ferhat Abbas, Setif 19000, Algeria
[4] Laboratory for Elaboration of New Materials and Characterization (LENMC), University Ferhat Abbas, of Setif 19000, Algeria
[5] Physics department, Faculty of sciences, Ain Shams University, Cairo, Egypt.
[6] Physics department, Faculty of sciences, Taif University, KSA
*E-mail: fatmimessaoud@yahoo.fr

Received June 9, 2010

We present structural, elastic, electronic, optical and thermal properties of the cubic structure Ni_3Al for various pressures. The computational method is based on the pseudo-potential plane wave (PP-PW). The exchange-correlation energy is described in both *generalized gradient approximation* (GGA) and the *local-density approximation* (LDA). The calculated equilibrium lattice parameter is in a reasonable agreement with the available experimental data. The value of Debye temperature obtained using elastic constants is about 466.49 K. Applied pressure does not change the shape of the total valence electronic charge density. The Fermi level is located in the part where the nickel contribution is very strong. Most of the electronic charge density is shifted toward Ni atoms. The coefficients of electronic and lattice heat capacities were calculated. Furthermore, in order to understand the optical properties of Ni_3Al, the dielectric function, absorption coefficient, refractive index and extinction coefficient are calculated for radiation up to 80 eV.

Key words: intermetallics; structural properties; electronic band structure; elastic properties; high pressure.

1. INTRODUCTION

Binary intermetallic compounds that contain a transition metal and a group-III metal display interesting electronic and magnetic properties. The Ni_3Al compound is of particular interest also from a magnetic point of view, as it displays weak itinerant ferromagnetism with a Curie temperature for the stoichiometric composition of 41.5 K [1]. This intermetallic compound provides a class of systems exhibiting unique mechanical properties that make them attractive for

structural applications [2]. This class of intermetallic alloys is very promising materials for high temperature and pressure applications and currently, it is being examined for use in diesel engine turbocharger rotors, high-temperature die and molds, hydroturbines, and cutting tools [3]. The structural and elastic properties were studied by *ab initio* within (FLMTO) method at lower pressure [2, 4]. The use of first principles calculations offers one of the most powerful tools for carrying out theoretical studies of an important number of physical and chemical properties of the condensed matter with great accuracy [5, 6]. In this work, we will contribute to the investigation of the Ni_3Al by performing a first principles study of its structural, elastic, electronic and thermodynamic properties.

The letter is organized as follows: in section 2, we briefly described the computational techniques used in this work. Results and discussions of our study will be presented in section 3. Finally, conclusions and remarks are given in section 4.

2. COMPUTATIONAL METHOD

The first-principles calculations were performed using a pseudo-potential plane-wave (PP-PW) method as implemented in CASTEP code [7]. Interactions of valence electrons with ion cores were represented by the Vanderbilt-type ultra soft pseudo-potential [8]. The exchange-correlation potential was calculated within the local density approximation (LDA) developed by Ceperley and Alder and parameterized by Perdew and Zunger [9, 10], as well as the generalized gradient approximation (GGA) of Perdew, Burke and Ernzerhof [11].

The plane-wave basis set cut-off was set as 660 eV. The special points sampling integration over the Brillouin zone was employed by using the Monkhorst-Pack method [12], with a 8x8x8 special *k*-point mesh. These parameters are sufficient in leading to well converged total energy, geometrical configurations and elastic moduli. The structural parameters of Ni_3Al were determined using the Broyden–Fletcher–Goldfarb–Shanno (BFGS) minimization technique [13], which provides a fast way to find the lowest energy structure.

The geometry optimization tolerance was selected as the difference of total energy within 5 x 10^{-6} eV per. atom, maximum ionic Hellmann-Feynman force within 0.01 eV/Å, maximum stress within 0.03 GPa and maximum ionic displacement within 10^{-4}Å. The elastic coefficients were determined from first-principles calculations by applying a homogeneous deformation with a finite value and calculating the resulting stress with respect to optimizing the internal atomic degrees of freedom [14]. The optical properties may be attracted from the knowledge of the complex dielectric function $\varepsilon(\omega) = \varepsilon_1(\omega) + i\,\varepsilon_2(\omega)$. The imaginary part was calculated from the momentum matrix elements between the occupied and unoccupied wave functions within the selection rules. The real part of dielectric function follows from the Kramer-Kronig relationship. There are two contributions to $\varepsilon(\omega)$, namely, intraband and interband transitions. The contribution from intraband is important only for metals. The interband transitions can further be split

into direct and indirect transitions. Optical constants such as the refractive index $n(\omega)$, extinction coefficient $k(\omega)$ and absorption coefficient $\alpha(\omega)$ may be computed from the values of $\varepsilon(\omega)$.

3. RESULTS AND DISCUSSIONS

3.1. STRUCTURAL PROPERTIES

The Ni_3Al compound has ideal cubic structure (SG: Pm-3m), where the atomic positions in the elementary cell are: Ni: 1a (0.5, 0.5, 0) and Al: 1a (0, 0, 0) as depicted in Fig. 1. The calculated structural properties of Ni_3Al using (PP-PW) method are summarized in Table 1, along with the available experimental and theoretical data. Our computed equilibrum lattice constants are determined by fitting the total energy as a function of the normalized volume to the Murnaghan (EOS). Our calculated equilibrum lattice parameter within GGA approach is in good agreement with others theoretical data quoted in ref. [2, 3, 15]. When comparing the results obtained within GGA (LDA), the computed lattice constant a deviates from the measured one cited in ref. [16] within 0.2 (2.3) %. The calculated unit cell volumes at fixed values of applied hydrostatic pressure in the range from 0 to 40 GPa were used to construct the equation of state (EOS) for Ni_3Al, which were fitted to a third order Birch-Murnaghan equation [17] Fig. 2:

$$P = \frac{3}{2} B_0 \left[\left(\frac{V}{V_0} \right)^{-7/3} - \left(\frac{V}{V_0} \right)^{-5/3} \right] \left[1 + \frac{3}{4} \left(B' - 4 \right) \left\{ \left(\frac{V}{V_0} \right)^{-2/3} - 1 \right\} \right]$$

Where B_0 is the bulk modulus, B' is the pressure derivative and V_0 fixed at the value determined from the zero pressure data. Least-squares fitting results in B_0 and B' at zero pressure are reported in Table 1. It seen that the normalized volume V/V_0 decreases monotonously with increasing pressure. If we refer to the experimental data, the value given by GGA is in good agreement than that of LDA.

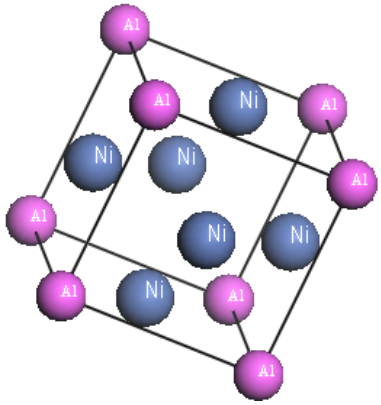

Fig. 1 – The cubic structure of Ni_3Al.

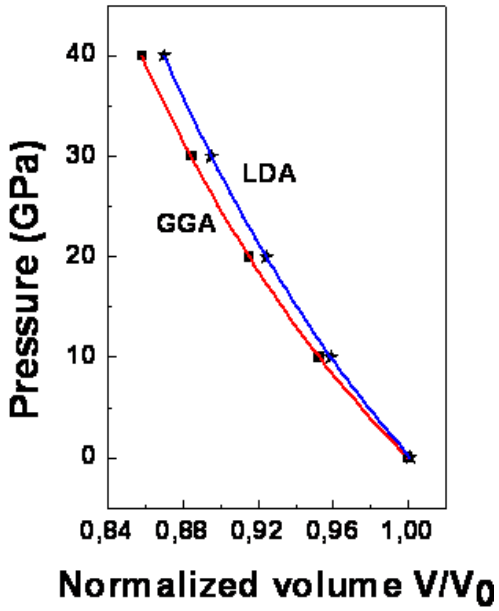

Fig. 2 – The calculated pressure *vs* normalized volume for Ni_3Al. The solid lines are given by the Birch-Murnaghan equation of state with the parameters listed in Table 1.

3.2. ELASTIC PROPERTIES

The elastic constants are important parameters that describe the response to an applied macroscopic stress. In Table 1, the calculated elastic constants, bulk modulus and first pressure derivatives of Ni_3Al are presented. Our results and those cited in Ref. [4] are in reasonable agreement. We next study the pressure dependence of the elastic properties. In Fig. 3, we present the variation of the elastic moduli of Ni_3Al with respect to the variation of pressure. We observe a linear dependence in all curves in the considered range of pressure. It is easy to observe that the elastic constants C_{ij} and bulk modulus B increase when the pressure is enhanced. Moreover, we can note that for the same pressure, the values of C_{ij}, bulk modulus and $\partial C_{ij}/\partial P$ given by LDA are greater than those given by GGA. The mechanical stability requires the elastic constants satisfying the well-known born stability criteria [18]:

$$K = \frac{1}{3}(C_{11} + 2C_{12} + P) > 0\,,\; G = \frac{1}{2}(C_{11} - C_{12} - 2P) > 0 \text{ and } G' = C_{44} - P > 0$$

In Fig. 4, we show the dependence of stability criteria of Ni_3Al compound with pressure. From our calculated C_{ij}, it is known that this compound is mechanically stable.

Table 1

The calculated lattice constant a_0, bulk modulus B, pressure derivative B', elastic constants C_{11}, C_{12} and C_{44}, shear modulus G, Young's modulus E, Poissons's ratio σ, anisotropy factor A and first pressure derivatives of elastic moduli

	Present work		Experiment	Other works
	GGA	LDA		
a_0(Å)	3.5609	3.4862	[a]3.572	[b]3.58
B_0 (GPa)	184.49	223.02	[a]171	[b]234
B'	4.520	4.560	-	-
C_{11}	230.31	276.92	-	[a]230
C_{12}	162.51	195.51	-	[a]139
C_{44}	124.79	146.71	-	[a]124.79
G	73.05	88.09	-	-
E	196.65	233.45	-	-
σ	0.320	0.32	-	-
A	0.78	0.76	-	-
□C_{11}/□P	4.83	4.25	-	-
□C_{12}/□P	4.25	4.49	-	-
□C_{44}/□P	2.33	2.24	-	
□B/□P	4.45	4.74		

[a]Ref. [4]
[b]Ref. [2]

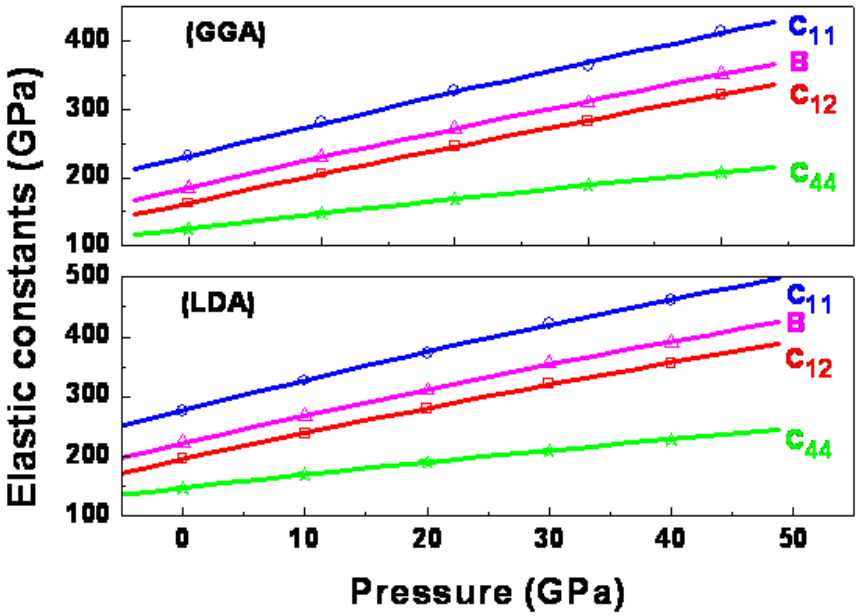

Fig. 3 – Elastic constants C_{11}, C_{12}, C_{44} and bulk modulus B of Ni_3Al using GGA and LDA calculations.

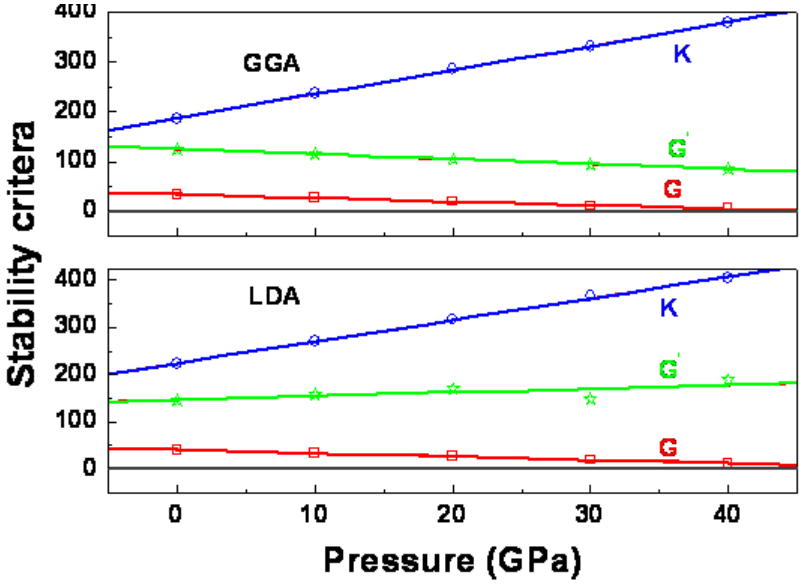

Fig. 4 – Stability criteria of Ni_3Al for both GGA and LDA calculations.

From the theoretical elastic constants, we computed the elastic wave velocities. The single-crystal elastic wave velocities in different directions are given by the resolution of the Cristoffel equation [19]:

$$\left(C_{ijkl}.n_j.n_k - \rho v^2.\delta_{il}\right).u_l = 0$$

where, C_{ijkl} is the single-crystal elastic constant tensor, n is the propagation direction, ρ is the density of material, u is the wave polarisation and v is the wave velocity. The solutions of this equation are of two types: a longitudinal wave with polarisation parallel to the direction of propagation v_l and two shear waves v_{T1} and v_{T2} with polarisation perpendicular to n. Another important parameter is the elastic anisotropy factor, A, which gives a measure of the anisotropy of the elastic wave velocity in a crystal. In a cubic crystal, the elastic anisotropy factor is given by [20]:

$$A = \frac{2C_{44} + C_{12}}{C_{11}} - 1$$

which is zero for an isotropic material. Any value smaller or larger than 0 indicates anisotropy. The magnitude of the deviation from 0 measures the degree of elastic anisotropy possessed by the crystal. We can observe that the anisotropy in the crystal is slightly smaller with GGA compared to that of LDA.

The calculated elastic wave velocities along the [100], [110] and [111] directions for Ni_3Al compound at zero pressure are shown in Table 2. At zero pressure, longitudinal waves are fastest along [111] and shear waves are slowest along [110] for Ni_3Al, which has a positive elastic anisotropy factor. The LDA gives elastic wave velocities greater than those of GGA.

Table 2

The calculated elastic wave velocities along the [100], [110] and [111] directions for Ni_3Al compound at zero pressure

Direction	v_L		v_{T1}		v_{T2}	
	LDA	GGA	LDA	GGA	LDA	GGA
[100]	5889	5552	4293	4087	4293	4087
[110]	6936	6557	2261	2130	4293	4087
[111]	7249	7112	3090	3039	3090	3039

Once the elastic constants are determined, we would like to compare our results with experiments, or predict what experiment would yield for the elastic constants. For cubic systems, the isotropic bulk modulus B is given exactly by:

$$B = \frac{C_{11} + 2C_{12}}{3}$$

The bounds on the shear modulus are given by:

$$G_R = \frac{5C_{44}\left(C_{11} - C_{12}\right)}{4C_{44} + 3\left(C_{11} - C_{12}\right)}$$

$$A = \frac{C_{11} - C_{12} + 3C_{44}}{5}$$

We also calculated Young's modulus E and Poisson's ratio σ which are frequently measured for polycrystalline materials when investigating their hardness. These quantities are related to the bulk modulus and the shear modulus by the following equations [21]:

$$E = \frac{9BG}{3B + G}$$

$$\sigma = \frac{3B - E}{6B}$$

The shear modulus $G = (G_R + G_V)/2$, Young's modulus E and Poisson's ratio σ for Ni_3Al compound, calculated from the elastic constants are listed in Table 1 The values of shear modulus given by LDA are greater than those given by GGA. Moreover, these approaches give practically the same value for Young's modulus and Poisson's ratio.

3.3. CALCULATION OF DEBYE TEMPERATURE

Having calculated Young's modulus E, bulk modulus B and shear modulus G, one can calculate Debye temperature, which is an important fundamental parameter closely related to many physical properties such as elastic constants, specific heat and melting temperature. At low temperature, the vibrational excitation arises solely from acoustic mode. Hence, at low temperature, Debye temperature calculated from elastic constants is the same as that determined from specific heat measurements. One of the standard methods to calculate Debye temperature θ_D is from elastic data, since θ_D may be estimated from the average sound velocity v_m by the following equation [22]:

$$\theta_D = \frac{h}{k_B}\left(\frac{3n}{4\pi V_a}\right)^{1/3} \nu_m$$

where h, k_B and V_a are Plank's constant, Boltzmann's constant and the atomic volume. The average sound velocity in the polycristalline material is given by [23]:

$$\nu_m = \left[\frac{1}{3}\left(\frac{2}{\nu_l^2} + \frac{1}{\nu_t^3}\right)\right]^{-1/3}$$

where v_l and v_t are the longitudinal and transverse sound velocity of an isotropic aggregate obtained using the shear modulus G and the bulk modulus B from Navier's equation [21]:

$$\nu_l = \left(\frac{3B + 4G}{3\rho}\right)^{1/2} \quad \text{and} \quad \nu_l = \left(\frac{G}{\rho}\right)^{1/2}$$

The calculated sound velocities and Debye temperature as well as the density for Ni_3Al are given in Table 3. The longitudinal, transverse and average sound velocities and the Debye temperature given by GGA are greater than those given by LDA. Our Debye temperature value given by GGA is in good agreement with the value 462 K cited in ref. [24].

Table 3

The calculated sound velocities and Debye temperature as well as the density for Ni_3Al

	ρ (g cm^{-3})	v_l (ms^{-1})	v_t(ms^{-1})	v_m(ms^{-1})	Θ_D(K)
GGA	7.4696	6168.36	3154.39	3533.80	466.49
LDA	7.9598	6536.5	3226.54	3727.79	502.64

3.4. ELECTRONIC PROPERTIES

Now we discuss our results pertaining to the electronic properties of Ni_3Al *via* the energy bands and total valence electronic charge density. The calculated band structure of Ni_3Al along the higher symmetry directions Γ, M, R and X in the Brillouin zone using (GGA) approach are given in Fig. 5. It seen that there is no band gap at the Fermi level. Valence and conduction bands overlap significantly at Fermi level, as a result, Ni_3Al exhibit a metallic character.

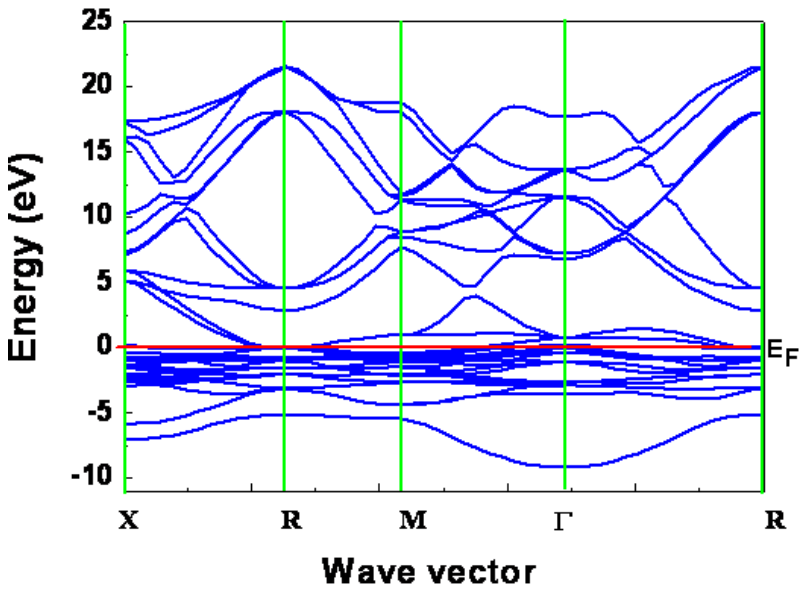

Fig. 5 – Band structure of Ni_3Al at equilibrium along the principal high-symmetry directions in the Brillouin zone.

The calculated (PDOS and TDOS) densities of states for Ni_3Al are shown in Fig. 6 within the energy interval from (E_F – 10 eV) up to (E_F +20 eV). In the region of the valence band, the width of the PDOS of Ni was clearly narrower than that of

Al. The number of Ni peaks was also less than that of Al. This indicates that the hybridization of Al 2p - Ni 3d is present. The density of states at the Fermi level of both nonmagnetic (NM) and ferromagnetic (FM) Ni_3Al are 5.813 and 3.27 states/eV/cell and the experiment value is about 11 states/eV/cell [25, 26]. Our value is about 5.5 states/eV/cell.

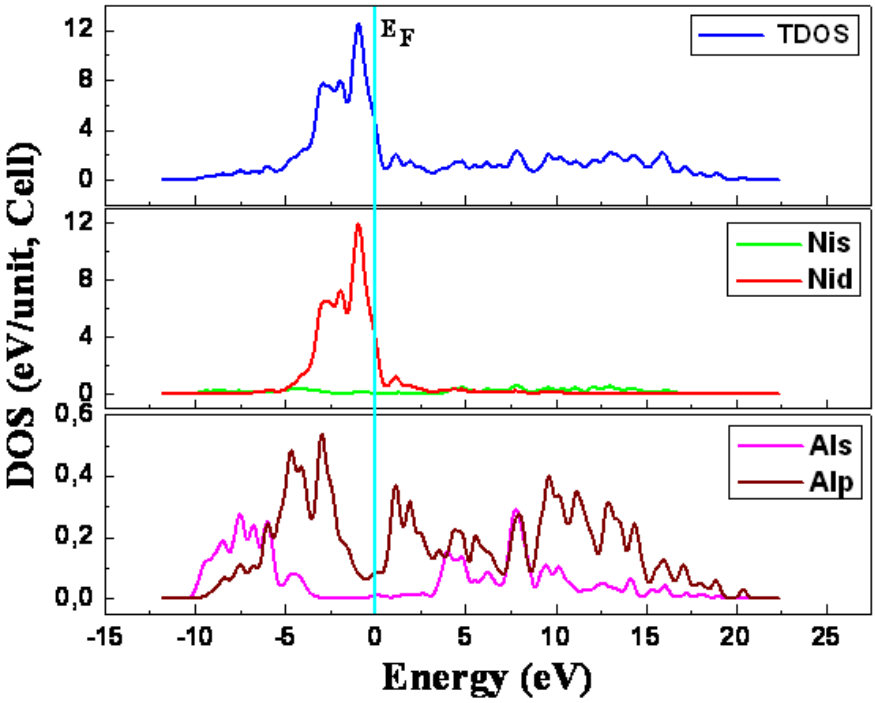

Fig. 6 – The calculated PDOS and TDOS for Ni_3Al, the Fermi level is set at zero energy and marked by vertical solid line.

The electronic valence charge density is a useful probe for the understanding of the chemical bonding in materials [27, 28]. In this work, the charge density is derived from a highly converged wave function. The Fig. 7 shows the computed total valence electron charge densities along the [110] direction for Ni_3Al using (GGA) under pressure. Note that most of the electronic charge density is shifted toward Ni atom. This is because Ni_3Al involves a charge transfer between the nearest neighbor's atoms. There is almost no charge in the interstitial region nearest the Al atom. A high degree of symmetry can be observed in the valence charge distribution. Applied pressure does not change the shape of the total valence electronic charge density. However, a remarkable enhancement of the charge density in the interatomic region is observed.

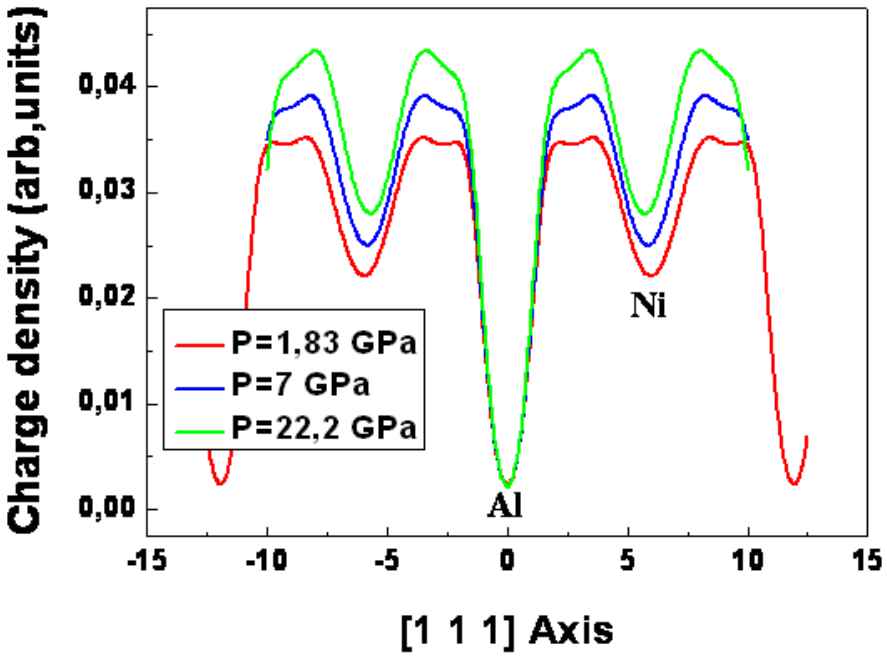

Fig. 7 – The total valence charge density for Ni_3Al at Γ point along [111] direction at different values of pressure.

The metallic properties of Ni_3Al can also be directly seen in Fig. 8, where the distribution of charge density on (110) plane gives detailed information on the interaction between atoms. Hybridization states Ni(d)–Al(p) clearly shows a strong covalent ionic-bonding between Ni and Al atoms. At the same time, the more electropositive nature of Al confirms the ionic bonding between Ni and Al. In order to give a deeper analysis on the bonding properties, we have calculated the overlap population for nearest neighbors in the crystal Table 4, positive and negative values being respectively related to bonding and antibonding states [29, 30]. We also performed the Mulliken charge population for Ni_3Al because it is a good method to understand bonding-behavior. The Mulliken population results are given in Table 4. The calculated Ni-Al and Ni-Ni bond length for Ni_3Al is 2.42 and 2.53 Å, respectively [16], which is close to our corresponding value of 2.517 Å for both Ni-Al and Ni-Ni bond length. In addition, high values of the unidirectional elastic modulus C_{11}, when compared to those of shear modulus C_{44} can be explained as follows: C_{11} is related to the bonding state of Al-Ni bonds along the principal crystal directions. However antibonding state of Ni-Ni bonds lead to a weaker resistance to shear deformation, *i.e.* weaker C_{44}.

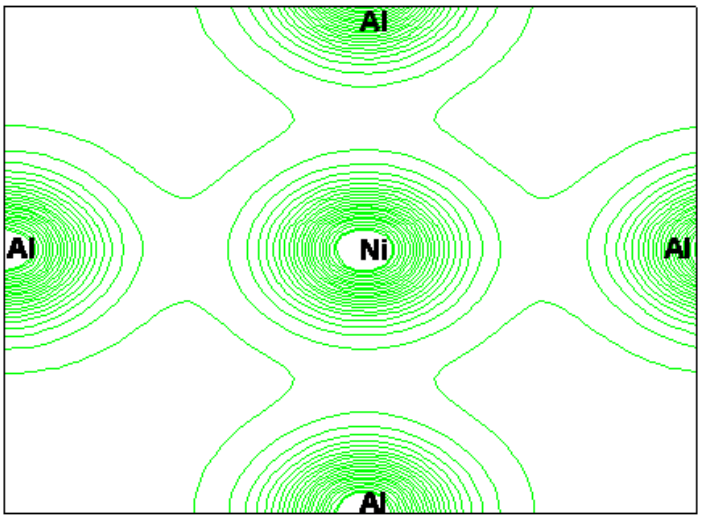

Fig. 8 – The total valence charge density for Ni_3Al calculated in (110) plane. The contours are given in units of electrons per unit cell.

Table 4

The Mulliken charge population for Ni_3Al crystal

Species	s	p	d	Total	Charge (electron)	Overlap population
Al	0.87	1.86	0	2.73	0.27	Ni-Ni (2.5179)
Ni	0.49	0.82	8.78	10.09	-0.09	Al-Ni (2.5179)

3.5. OPTICAL PROPERTIES

In order to account for the structures observed in the optical spectra, it is customary to consider transitions from occupied to unoccupied bands in the electronic energy band structure especially at high symmetry points in the Brillouin zone [31]. Based on the electronic structure, the dielectric function $\varepsilon(\omega) = \varepsilon_1(\omega) + i\,\varepsilon_2(\omega)$ of Ni_3Al were calculated. The $\varepsilon_2(\omega)$ and $\varepsilon_1(\omega)$ as function of photon energy are shown in (Fig. 9). We only considered the case of the incident radiation with the linear polarisation along the [100] direction. The imaginary part $\varepsilon_2(\omega)$ of the dielectric function is directly connected with the energy band structure. The top of the valence band VB and the bottom of the conduction band CB are composed of (Ni 3d) and (Al 3p) states. There is one peak located at 0.38 eV correspond to the transition (Ni 3d VB) to (Al 3p CB). It is noted that a peak in $\varepsilon_2(\omega)$ does not correspond to a single interband transition since many direct or indirect transitions may be found in band structure with an energy corresponding to the same peak [32]. The calculated static dielectric constant $\varepsilon_1(0) = 208.13$.

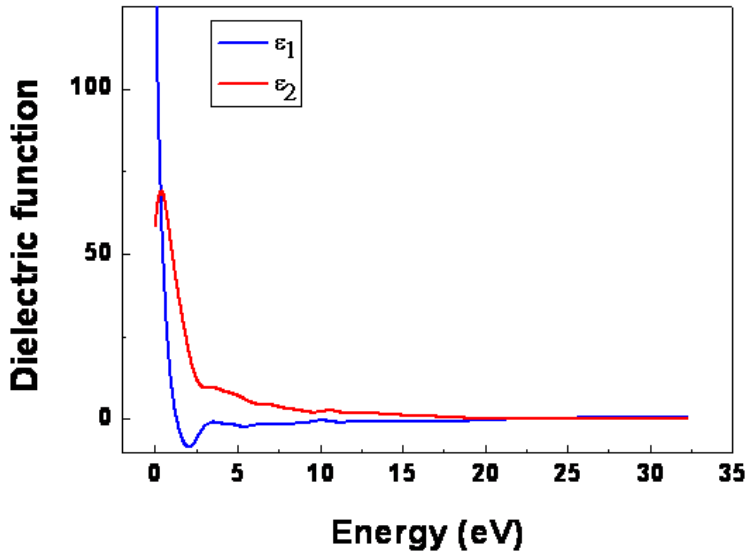

Fig. 9 – The calculated real part $\varepsilon_1(\omega)$ and imaginary part $\varepsilon_2(\omega)$ of the dielectric function $\varepsilon(\omega)$ for Ni_3Al.

The calculated results on the absorption spectrum, refractive index and extinction coefficient for Ni_3Al are shown in Figs. 10 and 11. In our calculation, we used Gaussian smearing that is 0.3 eV. The absorption spectrum started at 2.18 eV and reaches a maximum value at 14.93 eV. The calculated static refractive index is equal to 14.56.

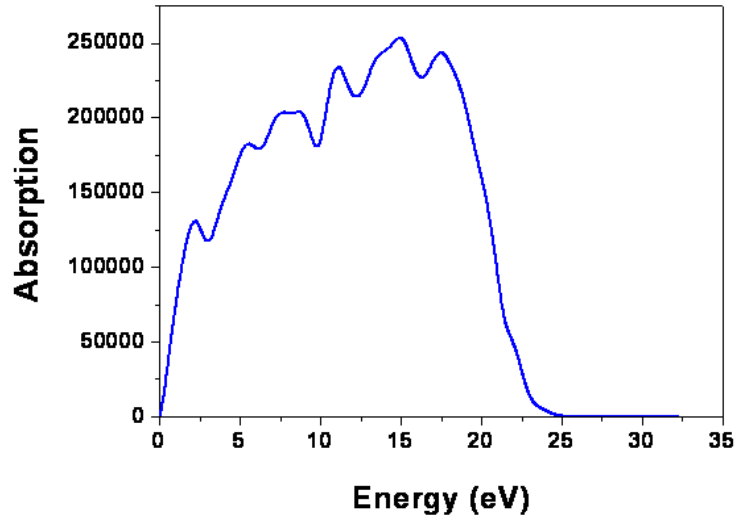

Fig. 10 – The calculated absorption coefficient $\alpha(\omega)$ for Ni_3Al.

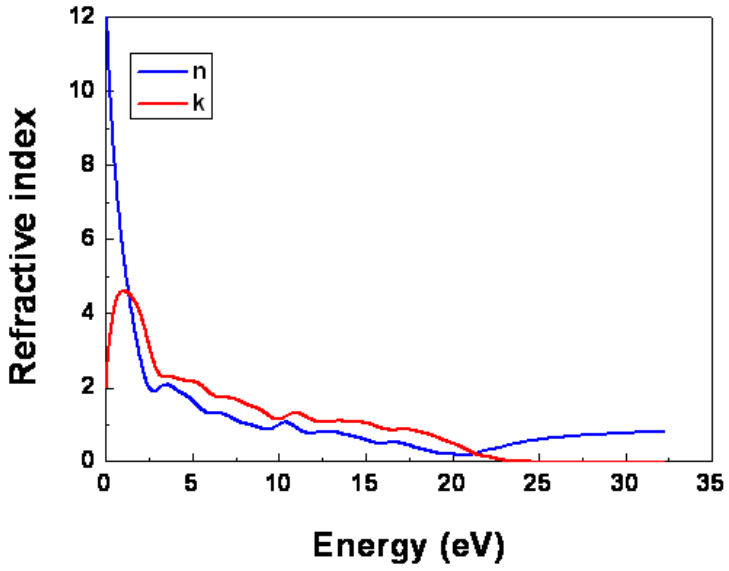

Fig. 11 – The calculated refractive index n(ω) and extinction coefficient k(ω) for Ni_3Al.

3.6. THERMAL PROPERTIES

We present in Fig. 12, the molar heat capacity of Ni_3Al as function of temperature. For temperatures lower than 20 K, the change of heat capacity is in T^3. This explains that only the acoustic modes with higher wave length are excited. Only, the modes treated as elastic continuum with macroscopic elastic constants intervene. At ambient temperature, the heat capacity is 21.33 Cal/mol.K and it reaches a plateau of 22.06 (*e.g.* $3Nk_B$) Cal/mol.K at higher temperatures. When replotted as C_P/T *vs* T^2 Fig. 13, a linear fit at the lower temperatures representing [33] $C_P/T = \gamma + \beta T^2$ as expected for a well behaved metallic-like system. The parameters γ and β are respectively, the coefficients of electronic and lattice heat capacities. A least squares fit of the linear segment yields $\gamma = 0{,}00133$ Cal/mol.K^2 and $\beta = 1{,}94591 \times 10^{-5}$ Cal/mol.K^4. The coefficient of lattice heat capacity, β, is related to the Debye temperature by [21]:

$$\theta_D^3 = n\left(\frac{12\pi^4 N k_B}{5\beta}\right)$$

where, n, N and k_B are, respectively, the number of atoms per molecule, Avogadro's number and Boltzmann's constant. Accordingly, with $n = 4$, a θ_D value of 463.6 K is obtained. This result is in good agreement with the $\theta_D = 457.5$ K at room temperature deduced from the Fig. 14 representing the variation of Debye temperature as a function of temperature. So, these results are in reasonable agreement with the values of Debye temperature calculated by elastic constants for

both (LDA) and (GGA) approaches and with the value 462 K cited in ref. [24]. The Debye temperature reaches a plateau of 458 K at higher temperatures. The plots of entropy, entalpy and free energy as a function of temperature are displayed in Fig. 15. The entropy and entalpy increase monotonously with increasing temperature. However, the free energy decreases monotonically with increasing temperature. The enhancement of entropy induced the disorder; moreover, the increasing in entalpy decreases the stability in this compound. At room temperature, the values of entalpy, entropy and free energy are 0.17, 0.31 and -0.14 eV respectively.

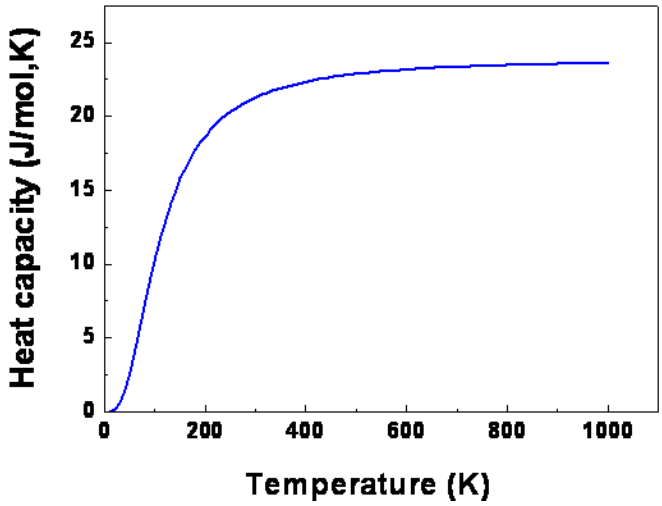

Fig. 12 – Temperature dependence of molar Heat capacity for Ni_3Al.

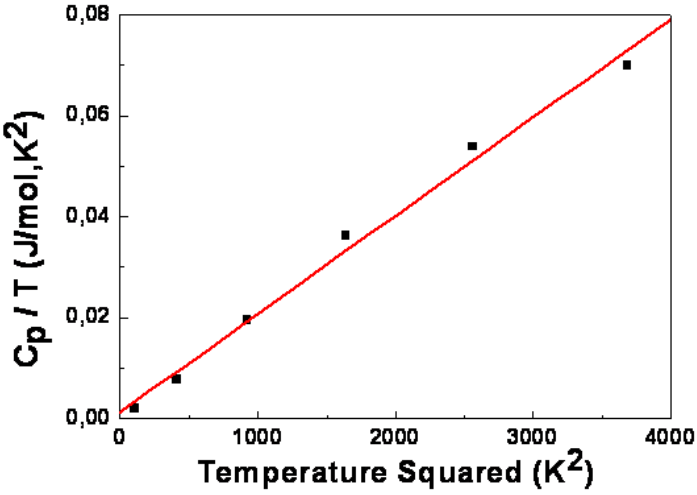

Fig. 13 - Plot of C_p /T *vs* T^2 for Ni_3Al at low temperatures.

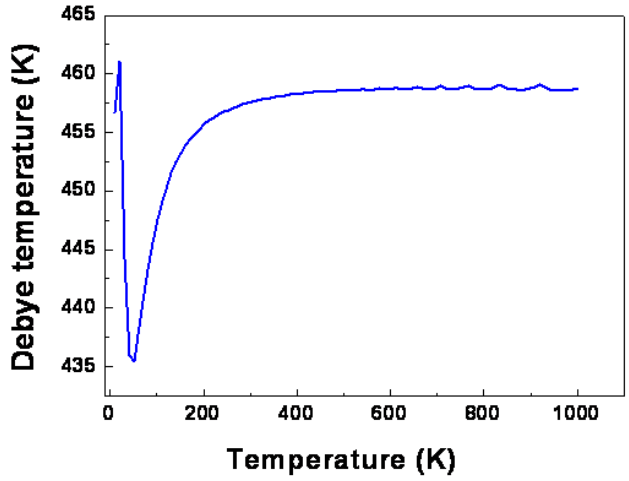

Fig. 14 – Temperature dependence of Debye temperature for Ni_3Al.

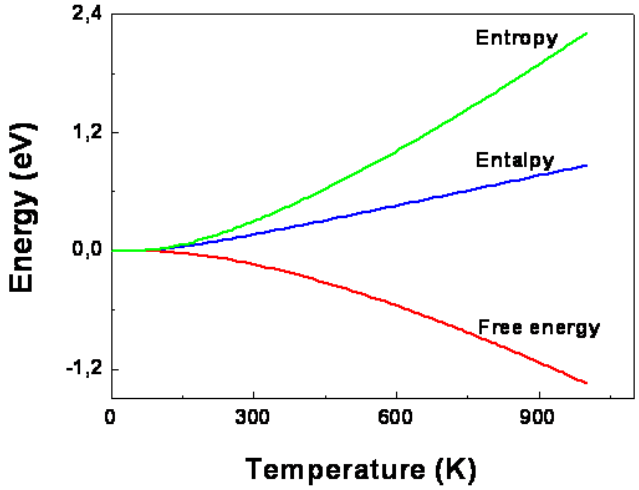

Fig. 15 – Plots of entropy, entalpy and free energy as function of temperature for Ni_3Al.

4. CONCLUSION

We have employed the pseudo-potential plane-wave (PP-PW) approach based on density functional theory, within the generalized gradient approximation (GGA) and the local density approximation (LDA). We have presented a study of structural, electronic, elastic optical and thermal properties of Ni_3Al. The calculated lattice constants at equilibrium are in reasonable agreement with the available experimental data. Debye temperature was calculated using elastic constants.

Bonding was discussed in the light of the electronic valence charge density. Applied pressure does not change the shape of the total valence electronic charge density. The dielectric function, absorption coefficient, refractive index and extinction coefficient are calculated for radiation up to 80 eV. Using the band structure, we have analyzed the interband contribution to the optical response functions.

REFERENCES

1. F. R. De Boer, C.J. Schinkel, J. Biesterbos, S. Proost , J. Appl. Phys., 40(1969) 1049.
2. Dobrina Iotova, Nicholas Kioussis, Say Peng Lim , Phys. Rev. B 54 (1996) 14413.
3. A. N. Mansour, A. Dmitrienko, A. V. Soldatov , Phys. Rev. B, Vol. 55 (23) (1997) 15531.
4. R. Sot, K. J. Kurzydlowski , Materials Science-Poland, 23 (2005) 587.
5. C. M. I. Okoye // J. Phys. : Condens. Matter 15 (2003) 5945.
6. R. L. Bernick, L. Kleinman // Solid State Commun. 8 (1970) 569.
7. M. D. Segall, P. J. D. Lindan, M. J. Probert, C. J. Pickard, P. J. Hasnip, S. J. Clark, M. C. Payne // J. Phys. Condens. Matter 14 (2002) 2717.
8. D. Vanderbilt // Phys. Rev. B 41 (1990) 7892.
9. D.M. Ceperley, B.J. Alder // Phys. Rev. Lett. 45 (1980) 566.
10. J.P. Perdew, A. Zunger // Phys. Rev. B 23 (1981) 5048.
11. J.P. Perdew, K. Burke, M. Ernzerhof // Phys. Rev. Lett. 77 (1996) 3865.
12. H.J. Monkhorst, J.D. Pack // Phys. Rev. B 13 (1976) 5188.
13. T.H. Fischer, J. Almlof // J. Phys. Chem. 96 (1992) 9768.
14. V. Milman, M.C. Warren // J. Phys. Condens. Matter 13 (2001) 241.
15. Li-Shing Hsu, Y.-K. Wang, G. Y. Guo // J. Appl. Phys. 92 (3) (1997) 1419.
16. Li-Shing Hsu, Y.-K. Wang, Y.-L. Tai, J.-F. Lee, Journal of Alloys and Compounds 413 (2006) 11.
17. F.D. Murnaghan // Proc. Nat1. Acad. Sci. USA 30 (1994) 244.
18. G. V. Sin'ko, A. Smirnov // J. Phys. Condens. Matter. 14 (2002) 6989.
19. B. Ghebouli, M.A. Ghebouli, M. Fatmi, S.I. Ahmed // Computational Materials Science 48 (2010) 94.
20. B. Ghebouli, M.A.Ghebouli, M.Fatmi, M. Benkerri // Computational Materials Science 48 (2010) 94.
21. M. W. Barsoum, T. El-Raghi, W. D. Porter, H. Wang, S. Chakraborty, // J. Appl. Phys. 88 (2000) 6313.
22. P. Wachter, M. Filzmoser, J. Rebisant // J. Physica B 293 (2001) 199.
23. O. L. Anderson // J. Phys. Chem. Solids 24 (1963) 909.
24. C. Costa, A. Biscarini, B. Coluzzi, F.M. Mazzolai, A.V. Granato // Materials Science and Engineering A192/193 (1995) 255.
25. G.Y. Guo, Y.K. Wang, Li-Shing Hsu // Journal of Magnetism and Magnetic Materials 239 (2002) 91.
26. Li-Shing Hsu, Y.-K. Wang, G. Y. Guo // J. Appl. Phys. 92 (3) (2002) 1419.
27. R. Hoffmann // Rev. Mod. Phys. 60 (1988) 601.
28. Z. Charifi, H. Baaziz, F. El. Hadj Hassan, N. Bouarissa // J. Phys. Condens. Matter 17 (2005) 4083.
29. M. D. Segall, R. Shah, C.J. Pickard, M.C. Payne // Phys. Rev B 54 (1996) 16317.
30. M. D. Segall, C.J. Pickard, R. Shah, M.C. Payne // Mol. Phys. 89 (1996) 571.
31. R. D. King-Smith, D. Vanderbilt // Phys. Rev. B 47 (1992) 1651.
32. A. Bouhemadou, R. Khenata // Comput. Mater. Sci. 39 (2007) 803.
33. S. E. Lofland, J. D. Hettinger, A. Bryan, P. Finkel, S. Gupta, M. W. Barsoum, G. Hug // Phys. Rev. B 74 (2006) 174501.